Short Article

Cell Stem Cell

Human Hippocampal Neurogenesis Persists throughout Aging

Graphical Abstract

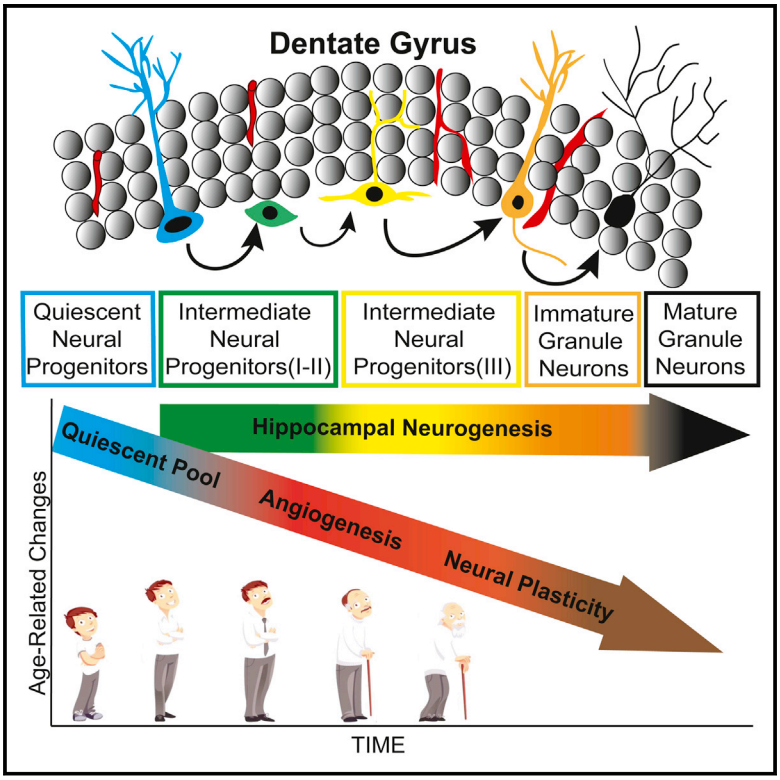

Authors

Maura Boldrini, Camille A. Fulmore, Alexandria N. Tartt, ..., Andrew J. Dwork, René Hen, J. John Mann

Correspondence

mb928@cumc.columbia.edu

In Brief

Boldrini et al. find persistent adult neurogenesis in humans into the eighth decade of life, despite declines in quiescent stem cell pools, angiogenesis, and neuroplasticity. Over a 65-year age span, proliferating neural progenitors, immature and mature granule neurons, glia, and dentate gryus volume were unchanged.

Highlights

- Pools of quiescent stem cells are smaller in aged human hippocampal dentate gyri
- Proliferating progenitor and immature neuron pools are stable with aging
- Angiogenesis and neuroplasticity decline in older humans
- Granule neurons, glia, and dentate gryus volume are unchanged with aging

Boldrini et al., 2018, Cell Stem Cell *22*, 589–599
April 5, 2018
https://doi.org/10.1016/j.stem.2018.03.015

CellPress

Cell Stem Cell
Short Article

Human Hippocampal Neurogenesis Persists throughout Aging

Maura Boldrini,[1,5,9,10,*] Camille A. Fulmore,[5] Alexandria N. Tartt,[5] Laika R. Simeon,[5] Ina Pavlova,[6] Verica Poposka,[8] Gorazd B. Rosoklija,[1,5,7] Aleksandar Stankov,[8] Victoria Arango,[1,5] Andrew J. Dwork,[1,2,5,7] René Hen,[1,3,4,6] and J. John Mann[1,5]

[1]Department of Psychiatry, Columbia University, New York, NY 10032, USA
[2]Department of Pathology and Cell Biology, Columbia University, New York, NY 10032, USA
[3]Department of Neuroscience, Columbia University, New York, NY 10032, USA
[4]Department of Pharmacology, Columbia University, New York, NY 10032, USA
[5]Division of Molecular Imaging and Neuropathology, NYS Psychiatric Institute, New York, NY 10032, USA
[6]Division of Integrative Neuroscience, NYS Psychiatric Institute, New York, NY 10032, USA
[7]Macedonian Academy of Sciences & Arts, 2, Ss. Cyril & Methodius University, Skopje 1000, Republic of Macedonia
[8]Institute for Forensic Medicine, Ss. Cyril & Methodius University, Skopje 1000, Republic of Macedonia
[9]Twitter: @DrMauraBoldrini
[10]Lead Contact
*Correspondence: mb928@cumc.columbia.edu
https://doi.org/10.1016/j.stem.2018.03.015

SUMMARY

Adult hippocampal neurogenesis declines in aging rodents and primates. Aging humans are thought to exhibit waning neurogenesis and exercise-induced angiogenesis, with a resulting volumetric decrease in the neurogenic hippocampal dentate gyrus (DG) region, although concurrent changes in these parameters are not well studied. Here we assessed whole autopsy hippocampi from healthy human individuals ranging from 14 to 79 years of age. We found similar numbers of intermediate neural progenitors and thousands of immature neurons in the DG, comparable numbers of glia and mature granule neurons, and equivalent DG volume across ages. Nevertheless, older individuals have less angiogenesis and neuroplasticity and a smaller quiescent progenitor pool in anterior-mid DG, with no changes in posterior DG. Thus, healthy older subjects without cognitive impairment, neuropsychiatric disease, or treatment display preserved neurogenesis. It is possible that ongoing hippocampal neurogenesis sustains human-specific cognitive function throughout life and that declines may be linked to compromised cognitive-emotional resilience.

INTRODUCTION

Healthy aging is crucial in a growing older population (United States Census Bureau, 2017). The ability to separate similar memory patterns (Sahay et al., 2011) and recover from stress (Schloesser et al., 2010) may depend on adult hippocampal neurogenesis (AHN), which is reported to decline with aging in nonhuman primates (Leuner et al., 2007) and mice (Ben Abdallah et al., 2007). New neurons are generated in the dentate gyrus (DG) of the adult human hippocampus, even after middle age (Eriksson et al., 1998), but the extent to which neurogenesis occurs in humans is highly debated and quantitative studies are scarce.

Phylogenetic differences between humans and rodents mandate assessment of the different stages of neuronal maturation in the human DG. For example, striatal neurogenesis is found only in humans (Bergmann et al., 2015), while olfactory bulb neurogenesis is absent in humans (Bergmann et al., 2012) but present in other mammals. Previous analyses of human AHN did not address the effects of aging, although studies have examined AHN in older populations (Eriksson et al., 1998). The density of doublecortin-positive (DCX+) cells were reported to decline from birth into the tenth decade of life (Knoth et al., 2010) in parallel with ^{14}C-determined neuron turnover (Bergmann et al., 2015); however, medication and drug use, which affect AHN (Boldrini et al., 2014), were not addressed (Knoth et al., 2010; Sorrells et al., 2018; Spalding et al., 2013). Using histological techniques that could not distinguish mature and immature neurons, several groups estimated that DG neurons did not decline in aging humans (Harding et al., 1998; Simić et al., 1997; West et al., 1994).

In vivo brain imaging studies reported conflicting findings regarding age-related changes in specific hippocampal regions. While some studies observed age-related declines in anterior hippocampal volume (Malykhin et al., 2008), others found no volume change (Head et al., 2005), or altered hippocampal shape rather than volume (Yang et al., 2013). Efforts to evaluate AHN *in vivo* face limitations due to inadequate spatial resolution and the inability to accurately differentiate hippocampal sub-regions (Ho et al., 2013; Manganas et al., 2007; Ramm et al., 2009).

AHN and angiogenesis are co-regulated (Boldrini et al., 2012; Heine et al., 2005; Thored et al., 2007; Warner-Schmidt and Duman, 2007). Exercise enhances cerebral blood volume, which results in more AHN in mice and better cognitive performance in humans (Pereira et al., 2007), but it may have a reduced impact in older people (Maass et al., 2015). Thus, we quantified AHN, angiogenesis, and DG volume and their relationship in people

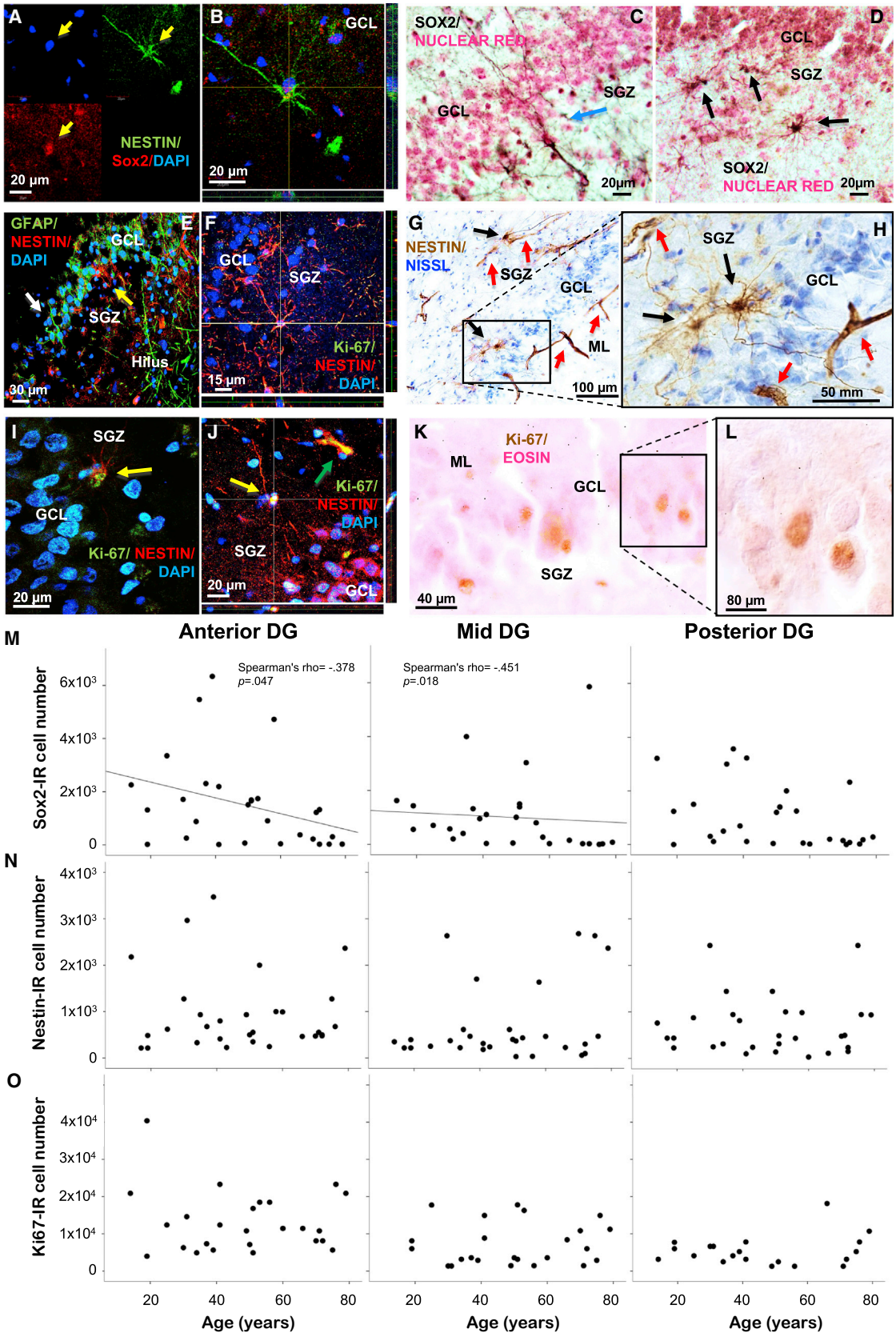

(legend on next page)

of different ages, hypothesizing that they would concurrently decrease with aging and correlate with each other.

Given the different functions of the rostral and caudal DG (Wu and Hen, 2014), we assessed the anterior, mid, and posterior hippocampus *postmortem* from 28 women and men 14 to 79 years of age. In each region, we characterized and quantified angiogenesis, volume, and cells at different maturational stages in the DG neurogenic niche, using unbiased stereological methods (West, 1993). To avoid confounders, subjects studied had no neuropsychiatric disease or treatment.

Healthy elderly people have the potential to remain cognitively and emotionally more intact than commonly believed, due to the persistence of AHN into the eighth decade of life. However, reduced cognitive-emotional resilience may be caused by a variety of factors such as a smaller quiescent neural progenitor pool, diminished angiogenesis, or decreasing neuroplasticity in the anterior DG.

RESULTS

The generation of new neurons in the DG neurogenic niche starts from quiescent radial-glia-like type I neural progenitor cells (QNPs) expressing glial fibrillary acid protein (GFAP), sex determining region Y-box 2 (Sox2), brain lipid-binding protein (BLBP), and nestin (Encinas et al., 2011). QNPs undergo asymmetric divisions and generate amplifying, or type II, intermediate neural progenitors (INPs) expressing Ki-67 and nestin (Encinas et al., 2011). As type II INPs differentiate into neuroblasts, or type III INPs, they lose the expression of Sox2 and GFAP while gaining expression of DCX and polysialylated neural cell adhesion molecule (PSA-NCAM), which is also expressed by immature and mature granule neurons (GNs) (Encinas et al., 2011). GNs are the final product of the differentiation cascade and express neuronal nuclear marker (NeuN), Prox-1, calbindin, and βIII-tubulin (Encinas et al., 2011). In anterior, mid, and posterior DG, we characterized and quantified the following: QNPs expressing GFAP, Sox2, and nestin; type I and II INPs expressing Ki-67 and nestin; neuroblasts, or type III INPs, and immature GNs expressing DCX and PSA-NCAM; and finally, mature GNs expressing NeuN. The anterior DG was defined as the portion from the most rostral appearance of the DG to the start of the lateral geniculate (visible in coronal brain sections); the mid DG spanned the lateral geniculate; and the posterior DG went from the end of the lateral geniculate to the caudal end of the DG.

QNPs Decline but INPs Are Stable during Human Aging

We assessed the first steps of neurogenesis, specifically the abundance of QNP and type I-II INP cells in the anterior, mid, and posterior DG of 28 males (n = 17) and females (n = 11) between 14 and 79 years of age. Expression of transcription factor Sox2, required for maintenance of multipotent neural stem cells (D'Amour and Gage, 2003), labeled QNPs and declined with aging selectively in anterior-mid DG, regardless of gender; GFAP also labeled QNPs, showing the typical radial-glia-like morphology, with apical processes (Figures 1A–1E, 1M, and S1A; Video S1). Sox2/nestin+ and nestin+ type I-II INPs (Yu et al., 2014) showed distinct perikaryon and multipolar processes, contacting nestin+ remodeling capillaries (Mokrý et al., 2008; Salehi et al., 2008) in the neurogenic niche of the subgranular zone (SGZ, Figures 1E–1H and Figures 4A–4C), as we reported earlier (Boldrini et al., 2009, 2012), and did not decline with age in human anterior, mid, or posterior DG in males or females (Figures 1N, S1B, and S1C). Nestin+ proliferating type II INPs also co-labeled with Ki-67, a marker of active cell cycle (Scholzen and Gerdes, 2000), and were found in the SGZ as seen in mice, and in the granule cell layer (GCL) (Figures 1F and 1I–1L), as we have shown in humans (Boldrini et al., 2012) and as others have found in nonhuman primates (Gould et al., 1999; Kornack and Rakic, 1999). Ki-67+ cells were stable between 14 and 79 years of age in human anterior, mid, and posterior DG in both sexes (Figure 1O).

In summary, the Sox2+ QNP pool was smaller in the anterior-mid DG of older people and comprised approximately 1,000 cells per DG region (anterior, mid, or posterior), while nestin+ and Sox2/nestin+ INP type I-II cells, in the range of thousands per DG region, were not fewer in older humans in anterior, mid, or posterior DG. Ki-67+ cells, unchanged between 14 and 79 years of age, were in the order of 10,000 per DG region, likely including dividing cells of non-neuronal lineage (likely endothelial and glial cells).

Immature GNs Are Preserved but Neuroplasticity Might Decline in Older Individuals

To test age-related changes in type II-III INPs and immature GNs, as well as activity-dependent neuroplasticity or migration, we used markers specific for this maturational phase.

PSA-NCAM was detected in neural cells with immature, bipolar, and pyramidal morphology and is considered a marker of neuroblasts or immature GNs only when co-labeled with DCX (Song et al., 2012); however, when found alone and on cells of different morphologies, it is considered a marker of neuroplasticity (Varbanov and Dityatev, 2017).

We found that PSA-NCAM+ cells in human SGZ, showing morphologies of INPs and immature GNs, and PSA-NCAM+ mature GNs were all fewer in anterior DG with older age, in

Figure 1. Fewer Quiescent Neural Progenitors and Stable Proliferating Intermediate Neural Progenitors in Aging Human Dentate Gyrus

(A and B) Co-expression of sex determining region Y-box 2 (Sox2) and nestin in QNPs; 4',6-diamidino-2-phenylindole (DAPI) stained nuclei.

(C) Sox2+ type I QNPs in the subgranular zone (SGZ) with apical processes crossing the granule cell layer (GCL) into the molecular layer (ML).

(D) Sox2+ type II INPs in SGZ.

(E) Glial fibrillary acid (GFAP)+ QNPs with apical process (white arrow) and hilar astrocytes and nestin+ INP (yellow arrow).

(F) Nestin/Ki-67+ INP.

(G and H) Nestin+ INPs (black arrows) and capillaries (red arrows); INP processes touch remodeling capillaries of tubular morphology.

(I and J) Nestin/Ki-67+ INPs (yellows arrows) and capillary (green arrow).

(K and L) Ki-67+ cells in SGZ/GCL and differential interference contrast image of Ki-67+ nuclei.

(M) Sox2+ cell decline in anterior-mid DG with aging.

(N and O) Nestin+ and Ki-67+ cells do not decline with older age in anterior, mid, or posterior DG.

both males and females, and had stable and cell-type-specific perikaryon volumes (Figures 2A–2G).

Conversely, we found stable numbers of DCX+ and DCX/PSA-NCAM+ cells across the 65-year age span in both genders (Figures 3A–3C, 3G, and S1D–S1F), representing preserved type III INP and immature GN numbers (Yu et al., 2014), which were in the order of a few thousands per DG region (anterior, mid, or posterior). Although we detected some DCX+ processes, they were rarely seen in adult human INPs (Figures 3A–3C and S1D; Video S2), as expected based on previous reports (Jin et al., 2004; Knoth et al., 2010). We confirmed PSA-NCAM/NeuN co-labeling, with most NeuN+ GNs not expressing PSA-NCAM (Figure 3D; Video S3).

We did not see an age-related decline of DCX+ and DCX/PSA-NCAM+ INPs and immature neurons, suggesting stable neurogenesis in older humans of both sexes. The finding of fewer PSA-NCAM+ cells of different morphologies ranging from type II INPs to mature neuron morphologies most likely represents a decline in neuroplasticity in aging humans, which could include blunted migration, dendrite sprouting, long-term potentiation, and activity-dependent plasticity.

Decreased Angiogenesis and Capillary Density in Aged Brains Correlates with Reduced Neuroplasticity while GN, Glia, and DG Volume Remain Unchanged

Here we report results related to angiogenesis measures, including the number of new capillaries per cubic mm, new capillary area and length, and the number of bifurcations per capillary, as well as the estimated total number of mature GNs and glia and DG volume, in the anterior, mid, and posterior hippocampal region from individuals 14 to 79 years of age.

Nestin is a marker of newly formed blood vessels (Boldrini et al., 2012; Salehi et al., 2008) and co-labels with collagen-IV, a vascular basement membrane marker, and platelet/endothelial cell adhesion molecule (PECAM, or CD31), a marker of endothelial cells (Boldrini et al., 2012). Nestin+ newly formed capillaries display distinct tube-like structure, clearly distinguishable from nestin+ INPs with a clear soma and processes (Figures 1G–1H and Figures 4A–4C). We assessed angiogenesis in anterior, mid, and posterior DG by measuring the length, area, and number of bifurcations of nestin+ remodeling capillaries and the number of new capillaries per mm^3 throughout the tissue section thickness (50 μm) using *Stereo Investigator* and *Neurolucida* software (MBF), as previously described (Boldrini et al., 2012; Salehi et al., 2008).

We estimated the volume of the anterior, mid, and posterior DG, including the volumes of GCL, molecular layer (ML), and SGZ, using the Cavalieri method (Simić et al., 1997), as previously reported (Boldrini et al., 2009, 2013). We aligned outlines of the DG including SGZ, GCL, and ML (Figure 3E) from the most rostral to the most caudal hippocampal sections (Video S4), and we used them to calculate the volume of the anterior, mid, and posterior DG and SGZ-GCL.

We found smaller total capillary area and length and shorter and less branched capillaries correlating with fewer PSA-NCAM+ cells selectively in anterior-mid DG (Figures 4D–4G and S2–S4). There was no correlation between a decline in capillary measures and the number of Sox2+, nestin+, Sox2/nestin+, Ki-67+, DCX+, DCX/PSA-NCAM+, NeuN+ cells, Nissl+ glia, or DG volume, regardless of gender (data not shown).

There was no age-related change in the number of NeuN+ GNs or Nissl+ glia estimated using stereology, nor in the volume of the DG or the GCL-SGZ in anterior, mid, and posterior hippocampus of both genders (Figures 3E–3F, 3H, and 3I and Figures 4H and 4I; Video S4), as estimated using the Cavalieri method (Boldrini et al., 2013).

There was an age-associated decline in angiogenesis in males and females, correlating with less neuroplasticity as represented by PSA-NCAM+ neuronal cells of different morphologies. Mature GN, glia, and DG volume were similar in people 14 to 79 years of age of both genders.

DISCUSSION

Aging effects on AHN, angiogenesis, and DG volume have not been studied concurrently in whole hippocampus *postmortem* from people with no neuropsychiatric disease or treatment and clear toxicology and neuropathology. In medication-free subjects with no brain disease and no reported cognitive impairment, good global functioning as per Global Assessment Scale (Endicott et al., 1976), and low recent (last 3 months) life event-related stress, quantified by St. Paul-Ramsey Life Experience Scale (Roy et al., 1986), we found persistent AHN into the eighth decade of life, and stable DG volume over a 65-year age span. In contrast, we found declining neuroplasticity and angiogenesis with older age, and a possibly diminished multipotent QNP pool selectively in anterior-mid DG, while the QNP pool remained unchanged in posterior DG, possibly reflecting less cognitive and emotional resilience with aging (Wu and Hen, 2014).

In aging individuals, our finding of fewer QNPs expressing Sox2+ and not nestin (D'Amour and Gage, 2003; Song et al., 2012), selectively in anterior-mid DG, agrees with mice data indicating a finite QNP pool undergoing asymmetric divisions that gets depleted over time (Encinas et al., 2011), or a self-renewing multipotent neural stem cell pool that, after symmetric self-renewal, undergoes terminal astrocytic differentiation (Bonaguidi et al., 2011). Nestin+ and Sox2/nestin+ cells in the order of about 1,000 per DG region (anterior, mid, or posterior) for a total of around 3,000 cells per DG at the time of death, in comparable amounts in younger and older individuals, suggest a constant proliferative potential of INPs that undertook the neuronal lineage. Moreover, the size of the INP pool is large enough to potentially have a relevant impact on the DG circuit if survival and maturation are warranted.

Ki-67+ cell numbers were in the order of 10,000 per DG region (anterior, mid, or posterior) for a total of around 30,000 per DG at the time of death with similar numbers in people 14 to 79 years of age, similarly to what we previously reported in individuals 17 to 53 years old (Boldrini et al., 2009), and consistent with findings of stable density of DG cells expressing proliferation markers across the human lifespan (Knoth et al., 2010). The number of Ki-67+ cells was 10-fold higher than the number of nestin+ and Sox2/nestin+ cells, suggesting that Ki-67+ cells possibly comprised proliferating cells of non-neuronal lineage (including endothelial and glial cells). Aging rhesus monkeys were found to have fewer DG proliferating cells and cognitive decline (Ngwenya et al., 2015), which was not seen in our sample.

Unchanged nestin+ and Sox2/nestin+ cells, representing type I-II INPs (Yu et al., 2014), in older age, with preserved Ki-67+ cell

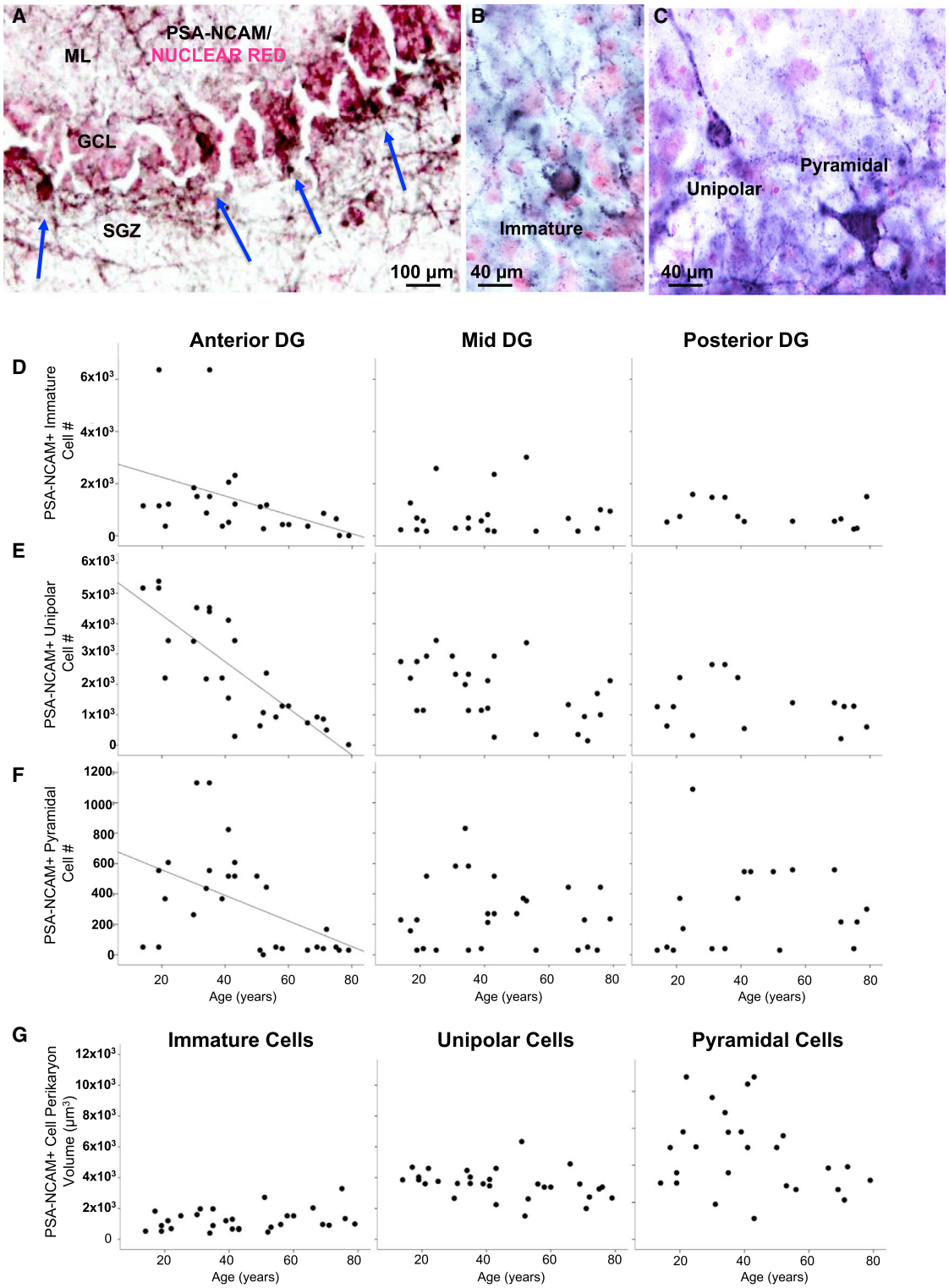

Figure 2. Fewer Polysialylated-Neural-Cell-Adhesion-Molecule-Positive Cells in Aging Human Dentate Gyrus

(A) PSA-NCAM+ cells in subgranular zone (SGZ) and granule cell layer (GCL) with processes projecting into the molecular layer (ML).

(B and C) PSA-NCAM+ cells of immature, unipolar, and pyramidal morphology.

(D–F) Fewer PSA-NCAM+ cells with aging in anterior DG.

(G) Immature, unipolar, and pyramidal cell soma volume is stable with aging.

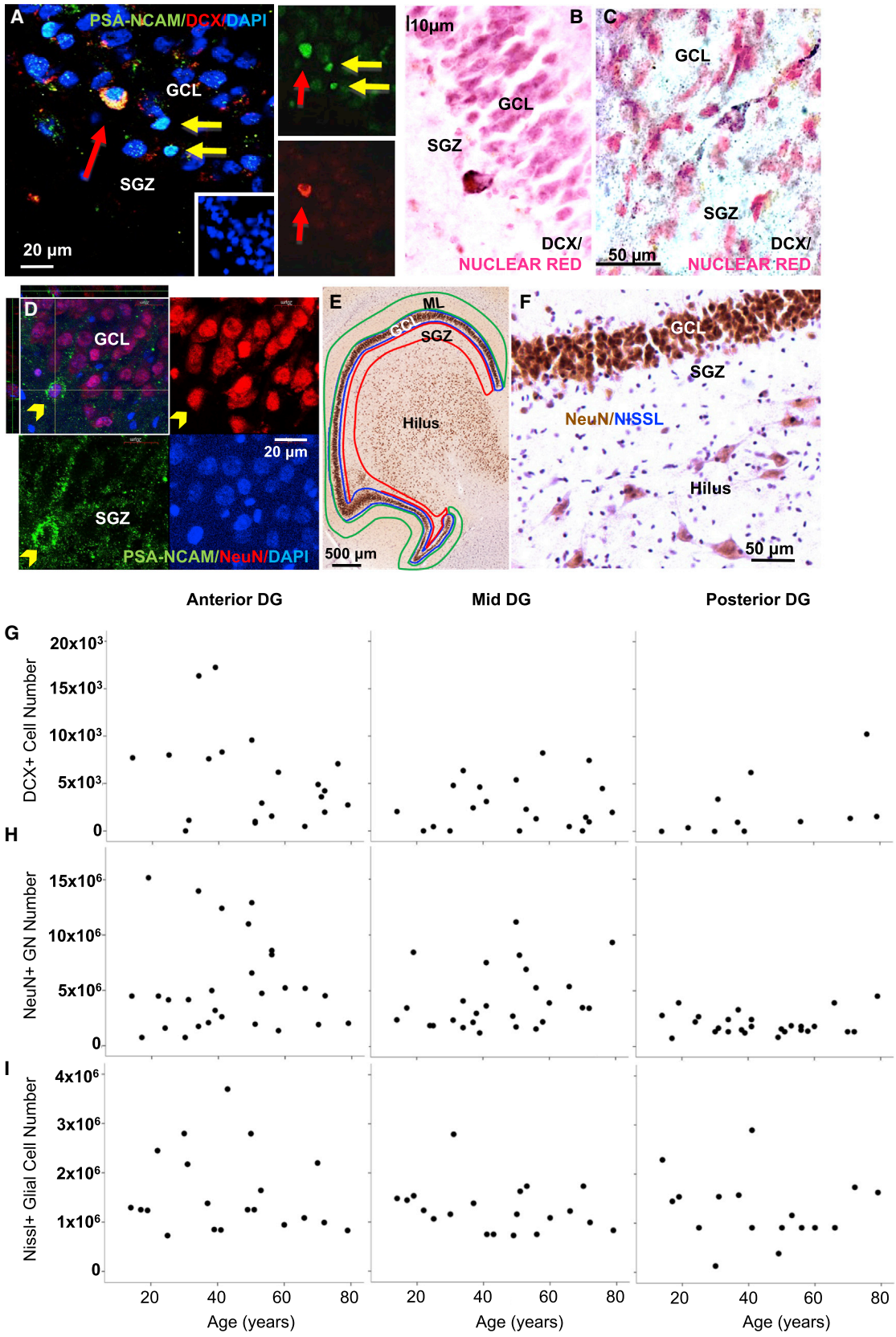

(legend on next page)

numbers, suggest maintained proliferative capacity in healthy aging, perhaps compensating for a smaller QNP pool as an adaptive response to age-associated social isolation in humans, given that in mice isolation boosted nestin+ cells (Dranovsky et al., 2011).

DCX+ and DCX/PSA-NCAM+ cells were stable with age and in the range of few thousands per DG region (anterior, mid, or posterior), for a total of 10,000–15,000 new INP type III, or immature neurons, per subject at one given time (the time of death). Others found that DCX+ cell density declined mainly between fetal and 15 years of age (Knoth et al., 2010), an age range that we did not study. Direct comparison between our data and Knoth's data is not possible because they analyzed only three 5 μm sections per subject from portions of the hippocampus, treated tissue at 80°C for 1 hr and at low pH to obtain deparaffinization and antigen retrieval, and assessed cell density without using stereology, which is the gold standard, given that cell density does not necessarily reflect total cell number (West and Gundersen, 1990). For the same reasons, we cannot compare our findings with those of a recent descriptive study that failed to detect DCX/PSA-NCAM+ cells in the DG from 15 subjects between 18 and 77 years of age (Sorrells et al., 2018).

Fewer PSA-NCAM+ cells with aging, with stable Sox2/nestin+ type II INPs and DCX/PSA-NCAM+ type III INPs or immature GNs, most likely indicate declining neuroplasticity or migration (Varbanov and Dityatev, 2017) rather than impaired INP proliferation, maturation, or survival. Moreover, we showed that a fraction of PSA-NCAM+ cells are NeuN+; therefore, a possible greater contribution of immature GNs, together with less mature GN neuroplasticity, would explain fewer PSA-NCAM+ and stable DCX/PSA-NCAM+ cells with aging. Assessing PSA-NCAM+ cells in DG/CA4 combined, without stereology, may account for the negative findings reported in 13 subjects 18 to 82 years of age, although the number of PSA-NCAM+ cells dropped between 3 and 18 years (Ní Dhúill et al., 1999).

A preserved number of NeuN+ mature GNs in anterior, mid, and posterior DG across ages agrees with earlier *postmortem* studies that used Hematoxylin/Eosin (Harding et al., 1998), Nissl (Simić et al., 1997), and Giemsa (West et al., 1994) stains and identified neurons solely based on morphology, finding age-related neuron loss in the following: CA1 (n = 12, age 46–85), driven by smaller whole-brain volume (Harding et al., 1998); CA1 and subiculum (n = 18, age 16–99) (Simić et al., 1997); and CA4 and subiculum (n = 38, only males, age 13–101) (West et al., 1994). It should be noted that fewer neurons in DG (Simić et al., 1997) and CA1 (West et al., 1994) were found in Alzheimer's disease patients. Spalding et al. (2013) also found fewer GNs with aging using cell sorting of homogenized tissue after dissecting the DG from other hippocampus subfields, an imprecise method, combined with potential unidentified psychiatric diagnoses.

Unchanged DG volume suggests that age-associated declines in DG/CA1–4 subfields found *postmortem* (Simić et al., 1997) and by *in vivo* neuroimaging (Daugherty et al., 2016) are likely due to smaller CA4, where fewer neurons were also reported (Harding et al., 1998).

In aging mice, more progenitors were found to undergo astrocytic differentiation (Encinas et al., 2011), and there were more astrocytes and microglia (Maurya and Mishra, 2017; Mouton et al., 2002). Therefore, our findings of unchanged numbers of Nissl+ glial cells in aging humans suggest that specific glial cell types should be assessed in aging human brain.

An age-related decline in anterior-mid DG angiogenesis in humans has not been previously reported. We found antidepressant-dependent correlation of angiogenesis (nestin+ capillaries) and type II INP proliferation (Boldrini et al., 2012), and now less angiogenesis correlated with fewer PSA-NCAM+ INPs and immature and mature GNs, possibly representing plasticity events, because PSA-NCAM+ cells were of different morphologies, and nestin/Sox2+ INPs, DCX/PSA-NCAM+ immature neurons, and NeuN+ GNs were not fewer with aging and their number did not correlate with angiogenesis measures. In agreement with our findings, exercise-induced increases in cerebral blood volume were blunted in older humans (60–77 years) compared with younger people (Maass et al., 2015), suggesting vascular niche signaling pathways (Heine et al., 2005; Thored et al., 2007; Warner-Schmidt and Duman, 2007) and blood-born factors (Katsimpardi et al., 2014) sustaining angiogenesis and cellular plasticity may decline with aging. The pathophysiology of age-associated brain diseases like Alzheimer's is linked to altered angiogenesis (Vagnucci and Li, 2003), microangiopathy (Perlmutter et al., 1990), and angiogenesis mediators that correlate with amounts of amyloid-β aggregates (Bridel et al., 2017). We were unable to assess exercise level, which enhances AHN, angiogenesis (Ekstrand et al., 2008), and hippocampal volume (Erickson et al., 2011), although it is likely that older individuals exercised less than younger people.

To minimize confounders, using our psychological autopsy (Kelly and Mann, 1996), clinical reports, brain and blood toxicology and neuropathology exams, we excluded subjects with neuropsychiatric and chronic diseases, microvascular changes (lacunae) or other neuropathology, psychotropic drug use, low tissue pH, and *postmortem* interval above 26 hr, to ensure uniformity of brain protein quality (Lewis, 2002). These methods are in part based on informant reporting, which is a key limitation in interpreting these data.

We did not detect differences in AHN levels or age-related changes between genders, and it should be noted that the

Figure 3. Preserved Immature and Mature Neurons and Glia in Aging Human Dentate Gyrus

(A) Polysialylated neural cell adhesion molecule (PSA-NCAM) and doublecortin (DCX) expression in an immature neuron between subgranular zone (SGZ) and granule cell layer (GCL), two PSA-NCAM+/DCX− cells, and 4',6-diamidino-2-phenylindole (DAPI)+ nuclei.

(B and C) DCX+ cells in SGZ, without and with stained processes.

(D) PSA-NCAM/NeuN+ cell with apical dendrite crossing the GCL.

(E) NeuN+ neurons in the granule cell layer (GCL), the molecular layer (ML), and subgranular zone (SGZ) are outlined; these outlines were used to calculate DG and GCL-SGZ volumes.

(F) NeuN+ neurons and Nissl+ glia in GCL and hilus.

(G–I) Stable DCX+ immature neurons, NeuN+ mature granule neurons, and Nissl+ glia.

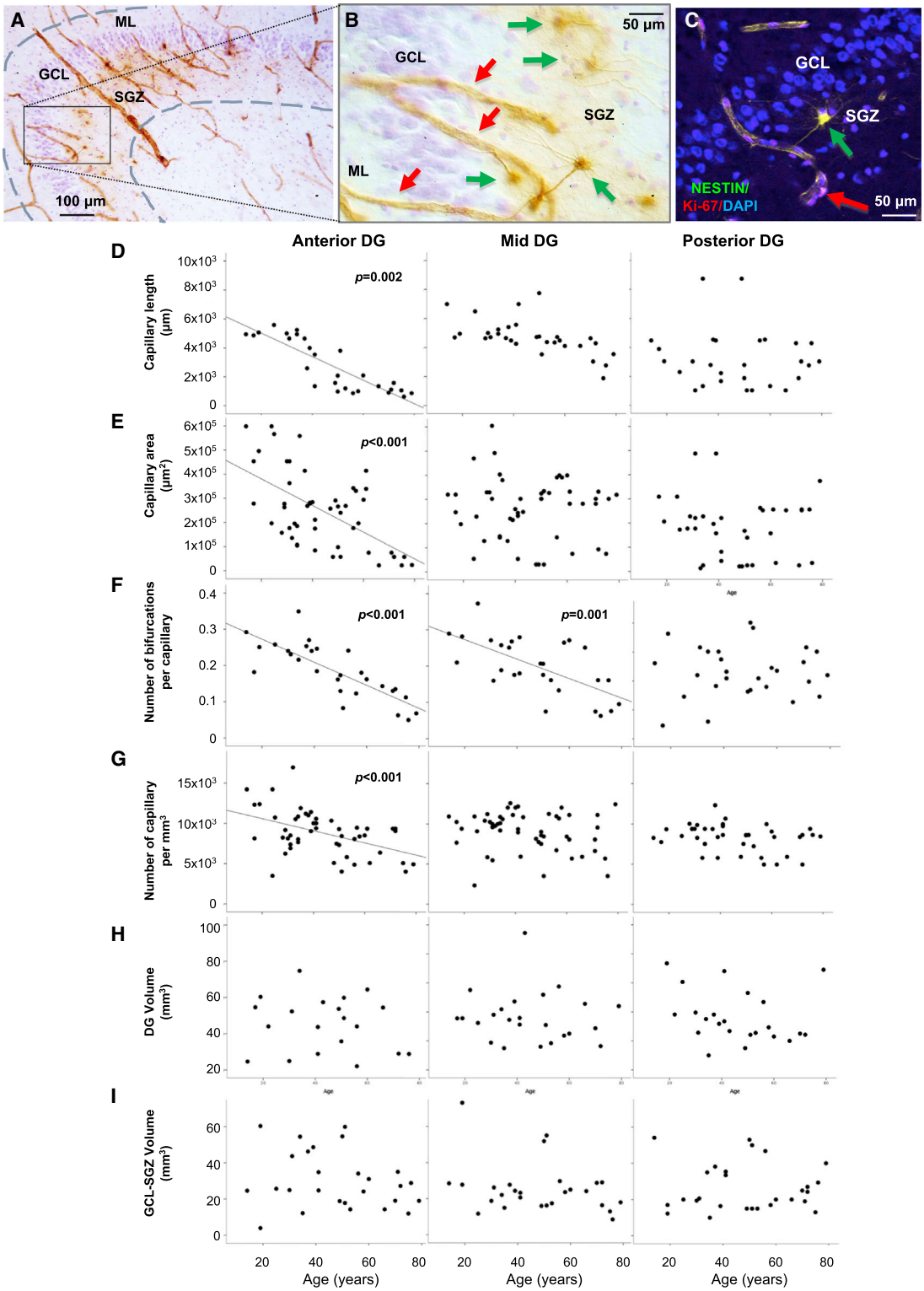

Figure 4. Age-Associated Dentate Gyrus Angiogenesis Decline and Stable DG Volume

(A) Nestin+ capillaries and neural progenitors and Nissl+ granule cells and glia; the outlined DG region was used to quantify cell numbers and DG volume.

(B) Differential interference contrast image of the quadrant in (A); nestin+ progenitors (green arrows) and capillaries (red arrows) are shown.

(C) Nestin/Ki-67+ progenitor (green arrow) and Ki-67+ endothelial cell (red arrow) in remodeling capillary; 4',6-diamidino-2-phenylindole (DAPI) stained nuclei.

(D–G) Fewer, shorter, less branched capillaries of smaller areas in anterior-mid DG occur with aging.

(H and I) DG and GCL-SGZ volumes are constant with aging.

women included in the study could have been in any phase of their menstrual cycle, while the older ones were probably in menopause, but such information was not available to us. It has been reported that hormones, including corticosteroids, estrogens, and testosterone, regulate neurogenesis and angiogenesis (Louissaint et al., 2002; McEwen, 2001; Saravia et al., 2007); therefore, the age-associated changes in angiogenesis, neuroplasticity, and multipotent progenitor pool that we are detecting may in part be due to different factors in women and men.

Older nonhuman primates and rodents have more GNs (Ngwenya et al., 2015; Kempermann et al., 2003) and less AHN (Ben Abdallah et al., 2007; Leuner et al., 2007) than younger ones, contrary to our findings in humans. Since new GNs may assist in pattern separation and old GNs in pattern completion (Aimone et al., 2011), steady AHN and concurrent elimination of older GNs likely supports human complex learning and memory and emotion-guided behavior throughout a long lifespan. Persistent AHN is vital for preserving cognitive flexibility and allowing memory-guided decision-making without the interference of irrelevant outdated information (Richards and Frankland, 2017). Our findings of thousands of new INPs and immature neurons (Sox2/nestin+ and DCX/PSA-NCAM+ cells) at the time of death, in anterior, mid, and posterior human SGZ, suggest that the number of newly generated neurons could be sufficient for them to have a relevant impact on the DG circuit. We only counted cells expressing specific markers at one time point, the time of demise, and expression of those markers may last a few weeks or months according to studies in primates (Kohler et al., 2011). It is hard to estimate the total number of new neurons generated in a few months or a year. Nevertheless, the estimate of about 700 new neurons in each human DG per day (Spalding et al., 2013) seems potentially consistent with our findings of a few thousand DCX/PSA-NCAM+ cells at time of death.

An exhausted quiescent progenitor pool, and less vascularization of the neurogenic niche resulting in less neuroplasticity, may explain some age-related cognitive-emotional changes. Future studies are needed to examine the cognitive and emotional correlates of these indices of neuroplasticity and the potential of exercise, diet, and medications to enhance healthy aging.

STAR★METHODS

Detailed methods are provided in the online version of this paper and include the following:

- KEY RESOURCES TABLE
- CONTACT FOR REAGENT AND RESOURCE SHARING
- EXPERIMENTAL MODEL AND SUBJECT DETAILS
  - Brain collection
  - Subject selection and matching procedure
  - Brain tissue processing
- METHOD DETAILS
  - Immunocytochemistry
  - Immunohistofluorescence
  - Replication
  - Confocal microscopy
  - Stereology
- QUANTIFICATION AND STATISTICAL ANALYSIS
- DATA AND SOFTWARE AVAILABILITY

SUPPLEMENTAL INFORMATION

Supplemental Information includes four figures, one table, and four videos and can be found with this article online at https://doi.org/10.1016/j.stem.2018.03.015.

ACKNOWLEDGMENTS

We thank the following: donors and families; teams performing psychological autopsy interviews; Yan Liu, Kelly M. Burke, Adrienne N. Santiago, Tanya H. Butt, Soo H. Kim, Manoj K. Jaiswal, and Cynthia Zizola for tissue processing, immunohistochemistry, stereology, and confocal microscopy; Mihran J. Bakalian for assistance with lab equipment and software; and Hanga Galfalvy for advice on statistical analyses. This work was supported by the following: the Stroud Center for Aging Studies at Columbia University; NIH grants MH83862, MH64168, MH40210, NS090415, MH94888, MH090964, and MH098786; American Foundation for Suicide Prevention SRG-0-129-12; Brain and Behavior Research Foundation Independent Investigator Grant 56388; New York Stem Cell Initiative C029157 and C023054; and the Diane Goldberg Foundation.

AUTHOR CONTRIBUTIONS

Conceptualization, M.B., J.J.M.; Methodology, M.B., C.A.F., L.R.S., A.N.T., I.P.; Investigation, M.B., C.A.F., L.R.S., A.N.T., I.P., V.P., A.S.; Validation, M.B., R.H., J.J.M.; Formal Analysis, M.B.; Writing – Original Draft, M.B.; Writing – Review & Editing, M.B., J.J.M., A.J.D., C.A.F., A.N.T., L.R.S., I.P., R.H.; Funding Acquisition, M.B., J.J.M., R.H., A.J.D., V.A.; Resources, A.J.D., G.B.R., J.J.M., V.P., A.S., V.A.; Supervision, M.B.

DECLARATION OF INTERESTS

A.J.D. received gifts from Olympus and Visiopharm; R.H. receives compensation as a consultant for Roche and Lundbeck; and J.J.M. receives royalties for commercial use of the C-SSRS from the Research Foundation for Mental Hygiene.

Received: July 13, 2017
Revised: September 24, 2017
Accepted: March 19, 2018
Published: April 5, 2018

REFERENCES

Aimone, J.B., Deng, W., and Gage, F.H. (2011). Resolving new memories: a critical look at the dentate gyrus, adult neurogenesis, and pattern separation. Neuron *70*, 589–596.

Ben Abdallah, N.M., Slomianka, L., and Lipp, H.P. (2007). Reversible effect of X-irradiation on proliferation, neurogenesis, and cell death in the dentate gyrus of adult mice. Hippocampus *17*, 1230–1240.

Bergmann, O., Liebl, J., Bernard, S., Alkass, K., Yeung, M.S., Steier, P., Kutschera, W., Johnson, L., Landén, M., Druid, H., et al. (2012). The age of olfactory bulb neurons in humans. Neuron *74*, 634–639.

Bergmann, O., Spalding, K.L., and Frisén, J. (2015). Adult Neurogenesis in Humans. Cold Spring Harb. Perspect. Biol. *7*, a018994.

Boldrini, M., Underwood, M.D., Hen, R., Rosoklija, G.B., Dwork, A.J., John Mann, J., and Arango, V. (2009). Antidepressants increase neural progenitor cells in the human hippocampus. Neuropsychopharmacology *34*, 2376–2389.

Boldrini, M., Hen, R., Underwood, M.D., Rosoklija, G.B., Dwork, A.J., Mann, J.J., and Arango, V. (2012). Hippocampal angiogenesis and progenitor cell proliferation are increased with antidepressant use in major depression. Biol. Psychiatry *72*, 562–571.

Boldrini, M., Santiago, A.N., Hen, R., Dwork, A.J., Rosoklija, G.B., Tamir, H., Arango, V., and John Mann, J. (2013). Hippocampal granule neuron number and dentate gyrus volume in antidepressant-treated and untreated major depression. Neuropsychopharmacology *38*, 1068–1077.

Boldrini, M., Butt, T.H., Santiago, A.N., Tamir, H., Dwork, A.J., Rosoklija, G.B., Arango, V., Hen, R., and Mann, J.J. (2014). Benzodiazepines and the potential trophic effect of antidepressants on dentate gyrus cells in mood disorders. Int. J. Neuropsychopharmacol. *17*, 1923–1933.

Bonaguidi, M.A., Wheeler, M.A., Shapiro, J.S., Stadel, R.P., Sun, G.J., Ming, G.L., and Song, H. (2011). In vivo clonal analysis reveals self-renewing and multipotent adult neural stem cell characteristics. Cell *145*, 1142–1155.

Bridel, C., Hoffmann, T., Meyer, A., Durieux, S., Koel-Simmelink, M.A., Orth, M., Scheltens, P., Lues, I., and Teunissen, C.E. (2017). Glutaminyl cyclase activity correlates with levels of Aβ peptides and mediators of angiogenesis in cerebrospinal fluid of Alzheimer's disease patients. Alzheimers Res. Ther. *9*, 38.

D'Amour, K.A., and Gage, F.H. (2003). Genetic and functional differences between multipotent neural and pluripotent embryonic stem cells. Proc. Natl. Acad. Sci. USA *100* (*Suppl 1*), 11866–11872.

Daugherty, A.M., Bender, A.R., Raz, N., and Ofen, N. (2016). Age differences in hippocampal subfield volumes from childhood to late adulthood. Hippocampus *26*, 220–228.

Dranovsky, A., Picchini, A.M., Moadel, T., Sisti, A.C., Yamada, A., Kimura, S., Leonardo, E.D., and Hen, R. (2011). Experience dictates stem cell fate in the adult hippocampus. Neuron *70*, 908–923.

Ekstrand, J., Hellsten, J., and Tingström, A. (2008). Environmental enrichment, exercise and corticosterone affect endothelial cell proliferation in adult rat hippocampus and prefrontal cortex. Neurosci. Lett. *442*, 203–207.

Encinas, J.M., Michurina, T.V., Peunova, N., Park, J.H., Tordo, J., Peterson, D.A., Fishell, G., Koulakov, A., and Enikolopov, G. (2011). Division-coupled astrocytic differentiation and age-related depletion of neural stem cells in the adult hippocampus. Cell Stem Cell *8*, 566–579.

Endicott, J., Spitzer, R.L., Fleiss, J.L., and Cohen, J. (1976). The global assessment scale. A procedure for measuring overall severity of psychiatric disturbance. Arch. Gen. Psychiatry *33*, 766–771.

Erickson, K.I., Voss, M.W., Prakash, R.S., Basak, C., Szabo, A., Chaddock, L., Kim, J.S., Heo, S., Alves, H., White, S.M., et al. (2011). Exercise training increases size of hippocampus and improves memory. Proc. Natl. Acad. Sci. USA *108*, 3017–3022.

Eriksson, P.S., Perfilieva, E., Björk-Eriksson, T., Alborn, A.M., Nordborg, C., Peterson, D.A., and Gage, F.H. (1998). Neurogenesis in the adult human hippocampus. Nat. Med. *4*, 1313–1317.

Gould, E., Reeves, A.J., Fallah, M., Tanapat, P., Gross, C.G., and Fuchs, E. (1999). Hippocampal neurogenesis in adult Old World primates. Proc. Natl. Acad. Sci. USA *96*, 5263–5267.

Harding, A.J., Halliday, G.M., and Kril, J.J. (1998). Variation in hippocampal neuron number with age and brain volume. Cereb. Cortex *8*, 710–718.

Harrison, P.J., Heath, P.R., Eastwood, S.L., Burnet, P.W.J., McDonald, B., and Pearson, R.C.A. (1995). The relative importance of premortem acidosis and postmortem interval for human brain gene expression studies: selective mRNA vulnerability and comparison with their encoded proteins. Neurosci. Lett. *200*, 151–154.

Head, D., Snyder, A.Z., Girton, L.E., Morris, J.C., and Buckner, R.L. (2005). Frontal-hippocampal double dissociation between normal aging and Alzheimer's disease. Cereb. Cortex *15*, 732–739.

Heine, V.M., Zareno, J., Maslam, S., Joëls, M., and Lucassen, P.J. (2005). Chronic stress in the adult dentate gyrus reduces cell proliferation near the vasculature and VEGF and Flk-1 protein expression. Eur. J. Neurosci. *21*, 1304–1314.

Ho, N.F., Hooker, J.M., Sahay, A., Holt, D.J., and Roffman, J.L. (2013). In vivo imaging of adult human hippocampal neurogenesis: progress, pitfalls and promise. Mol. Psychiatry *18*, 404–416.

Jin, K., Peel, A.L., Mao, X.O., Xie, L., Cottrell, B.A., Henshall, D.C., and Greenberg, D.A. (2004). Increased hippocampal neurogenesis in Alzheimer's disease. Proc. Natl. Acad. Sci. USA *101*, 343–347.

Katsimpardi, L., Litterman, N.K., Schein, P.A., Miller, C.M., Loffredo, F.S., Wojtkiewicz, G.R., Chen, J.W., Lee, R.T., Wagers, A.J., and Rubin, L.L. (2014). Vascular and neurogenic rejuvenation of the aging mouse brain by young systemic factors. Science *344*, 630–634.

Kelly, T.M., and Mann, J.J. (1996). Validity of DSM-III-R diagnosis by psychological autopsy: a comparison with clinician ante-mortem diagnosis. Acta Psychiatr. Scand. *94*, 337–343.

Kempermann, G., Gast, D., Kronenberg, G., Yamaguchi, M., and Gage, F.H. (2003). Early determination and long-term persistence of adult-generated new neurons in the hippocampus of mice. Development *130*, 391–399.

Knoth, R., Singec, I., Ditter, M., Pantazis, G., Capetian, P., Meyer, R.P., Horvat, V., Volk, B., and Kempermann, G. (2010). Murine features of neurogenesis in the human hippocampus across the lifespan from 0 to 100 years. PLoS ONE *5*, e8809.

Kohler, S.J., Williams, N.I., Stanton, G.B., Cameron, J.L., and Greenough, W.T. (2011). Maturation time of new granule cells in the dentate gyrus of adult macaque monkeys exceeds six months. Proc. Natl. Acad. Sci. USA *108*, 10326–10331.

Kornack, D.R., and Rakic, P. (1999). Continuation of neurogenesis in the hippocampus of the adult macaque monkey. Proc. Natl. Acad. Sci. USA *96*, 5768–5773.

Leuner, B., Kozorovitskiy, Y., Gross, C.G., and Gould, E. (2007). Diminished adult neurogenesis in the marmoset brain precedes old age. Proc. Natl. Acad. Sci. USA *104*, 17169–17173.

Lewis, D.A. (2002). The human brain revisited: opportunities and challenges in postmortem studies of psychiatric disorders. Neuropsychopharmacology *26*, 143–154.

Louissaint, A., Jr., Rao, S., Leventhal, C., and Goldman, S.A. (2002). Coordinated interaction of neurogenesis and angiogenesis in the adult songbird brain. Neuron *34*, 945–960.

Maass, A., Düzel, S., Goerke, M., Becke, A., Sobieray, U., Neumann, K., Lövden, M., Lindenberger, U., Bäckman, L., Braun-Dullaeus, R., et al. (2015). Vascular hippocampal plasticity after aerobic exercise in older adults. Mol. Psychiatry *20*, 585–593.

Malykhin, N.V., Bouchard, T.P., Camicioli, R., and Coupland, N.J. (2008). Aging hippocampus and amygdala. Neuroreport *19*, 543–547.

Manganas, L.N., Zhang, X., Li, Y., Hazel, R.D., Smith, S.D., Wagshul, M.E., Henn, F., Benveniste, H., Djuric, P.M., Enikolopov, G., and Maletic-Savatic, M. (2007). Magnetic resonance spectroscopy identifies neural progenitor cells in the live human brain. Science *318*, 980–985.

Maurya, S.K., and Mishra, R. (2017). Pax6 interacts with Iba1 and shows age-associated alterations in brain of aging mice. J. Chem. Neuroanat. *82*, 60–64.

McEwen, B.S. (2001). Plasticity of the hippocampus: adaptation to chronic stress and allostatic load. Ann. N Y Acad. Sci. *933*, 265–277.

Mokrý, J., Ehrmann, J., Karbanová, J., Cízková, D., Soukup, T., Suchánek, J., Filip, S., and Kolár, Z. (2008). Expression of intermediate filament nestin in blood vessels of neural and non-neural tissues. Acta Med. (Hradec Kralove) *51*, 173–179.

Mouton, P.R., Long, J.M., Lei, D.L., Howard, V., Jucker, M., Calhoun, M.E., and Ingram, D.K. (2002). Age and gender effects on microglia and astrocyte numbers in brains of mice. Brain Res. *956*, 30–35.

Ngwenya, L.B., Heyworth, N.C., Shwe, Y., Moore, T.L., and Rosene, D.L. (2015). Age-related changes in dentate gyrus cell numbers, neurogenesis, and associations with cognitive impairments in the rhesus monkey. Front. Syst. Neurosci. *9*, 102.

Ní Dhúill, C.M., Fox, G.B., Pittock, S.J., O'Connell, A.W., Murphy, K.J., and Regan, C.M. (1999). Polysialylated neural cell adhesion molecule expression in the dentate gyrus of the human hippocampal formation from infancy to old age. J. Neurosci. Res. *55*, 99–106.

Pereira, A.C., Huddleston, D.E., Brickman, A.M., Sosunov, A.A., Hen, R., McKhann, G.M., Sloan, R., Gage, F.H., Brown, T.R., and Small, S.A. (2007). An in vivo correlate of exercise-induced neurogenesis in the adult dentate gyrus. Proc. Natl. Acad. Sci. USA *104*, 5638–5643.

Perlmutter, L.S., Chui, H.C., Saperia, D., and Athanikar, J. (1990). Microangiopathy and the colocalization of heparan sulfate proteoglycan with amyloid in senile plaques of Alzheimer's disease. Brain Res. *508*, 13–19.

Ramm, P., Couillard-Despres, S., Plötz, S., Rivera, F.J., Krampert, M., Lehner, B., Kremer, W., Bogdahn, U., Kalbitzer, H.R., and Aigner, L. (2009). A nuclear magnetic resonance biomarker for neural progenitor cells: is it all neurogenesis? Stem Cells *27*, 420–423.

Richards, B.A., and Frankland, P.W. (2017). The Persistence and Transience of Memory. Neuron *94*, 1071–1084.

Roy, A., Pickar, D., Linnoila, M., Doran, A.R., and Paul, S.M. (1986). Cerebrospinal fluid monoamine and monoamine metabolite levels and the dexamethasone suppression test in depression. Relationship to life events. Arch. Gen. Psychiatry *43*, 356–360.

Sahay, A., Scobie, K.N., Hill, A.S., O'Carroll, C.M., Kheirbek, M.A., Burghardt, N.S., Fenton, A.A., Dranovsky, A., and Hen, R. (2011). Increasing adult hippocampal neurogenesis is sufficient to improve pattern separation. Nature *472*, 466–470.

Salehi, F., Kovacs, K., Cusimano, M.D., Horvath, E., Bell, C.D., Rotondo, F., and Scheithauer, B.W. (2008). Immunohistochemical expression of nestin in adenohypophysial vessels during development of pituitary infarction. J. Neurosurg. *108*, 118–123.

Saravia, F., Beauquis, J., Pietranera, L., and De Nicola, A.F. (2007). Neuroprotective effects of estradiol in hippocampal neurons and glia of middle age mice. Psychoneuroendocrinology *32*, 480–492.

Schloesser, R.J., Lehmann, M., Martinowich, K., Manji, H.K., and Herkenham, M. (2010). Environmental enrichment requires adult neurogenesis to facilitate the recovery from psychosocial stress. Mol. Psychiatry *15*, 1152–1163.

Scholzen, T., and Gerdes, J. (2000). The Ki-67 protein: from the known and the unknown. J. Cell. Physiol. *182*, 311–322.

Simić, G., Kostović, I., Winblad, B., and Bogdanović, N. (1997). Volume and number of neurons of the human hippocampal formation in normal aging and Alzheimer's disease. J. Comp. Neurol. *379*, 482–494.

Song, J., Christian, K.M., Ming, G.L., and Song, H. (2012). Modification of hippocampal circuitry by adult neurogenesis. Dev. Neurobiol. *72*, 1032–1043.

Sorrells, S.F., Paredes, M.F., Cebrian-Silla, A., Sandoval, K., Qi, D., Kelley, K.W., James, D., Mayer, S., Chang, J., Auguste, K.I., et al. (2018). Human hippocampal neurogenesis drops sharply in children to undetectable levels in adults. Nature *555*, 377–381.

Spalding, K.L., Bergmann, O., Alkass, K., Bernard, S., Salehpour, M., Huttner, H.B., Boström, E., Westerlund, I., Vial, C., Buchholz, B.A., et al. (2013). Dynamics of hippocampal neurogenesis in adult humans. Cell *153*, 1219–1227.

Thored, P., Wood, J., Arvidsson, A., Cammenga, J., Kokaia, Z., and Lindvall, O. (2007). Long-term neuroblast migration along blood vessels in an area with transient angiogenesis and increased vascularization after stroke. Stroke *38*, 3032–3039.

United States Census Bureau (2017). The Nation's Older Population Is Still Growing, Census Bureau Reports. Release Number: CB17-100. https://www.census.gov/newsroom/press-releases/2017/cb17-100.html.

Vagnucci, A.H., Jr., and Li, W.W. (2003). Alzheimer's disease and angiogenesis. Lancet *361*, 605–608.

Varbanov, H., and Dityatev, A. (2017). Regulation of extrasynaptic signaling by polysialylated NCAM: Impact for synaptic plasticity and cognitive functions. Mol. Cell. Neurosci. *81*, 12–21.

Warner-Schmidt, J.L., and Duman, R.S. (2007). VEGF is an essential mediator of the neurogenic and behavioral actions of antidepressants. Proc. Natl. Acad. Sci. USA *104*, 4647–4652.

West, M.J. (1993). New stereological methods for counting neurons. Neurobiol. Aging *14*, 275–285.

West, M.J., and Gundersen, H.J. (1990). Unbiased stereological estimation of the number of neurons in the human hippocampus. J. Comp. Neurol. *296*, 1–22.

West, M.J., Coleman, P.D., Flood, D.G., and Troncoso, J.C. (1994). Differences in the pattern of hippocampal neuronal loss in normal ageing and Alzheimer's disease. Lancet *344*, 769–772.

Wu, M.V., and Hen, R. (2014). Functional dissociation of adult-born neurons along the dorsoventral axis of the dentate gyrus. Hippocampus *24*, 751–761.

Yang, X., Goh, A., Chen, S.H., and Qiu, A. (2013). Evolution of hippocampal shapes across the human lifespan. Hum. Brain Mapp. *34*, 3075–3085.

Yu, D.X., Di Giorgio, F.P., Yao, J., Marchetto, M.C., Brennand, K., Wright, R., Mei, A., McHenry, L., Lisuk, D., Grasmick, J.M., et al. (2014). Modeling hippocampal neurogenesis using human pluripotent stem cells. Stem Cell Reports *2*, 295–310.

STAR★METHODS

KEY RESOURCES TABLE

REAGENT or RESOURCE	SOURCE	IDENTIFIER
Antibodies		
Rabbit anti-Sox2	Millipore	Cat# AB5603 RRID:AB_2286686
Novocastra Liquid Mouse Monoclonal Antibody Ki67 Antigen	Leica Biosystems	Product Code: NCL-L-Ki67-MM1
Mouse anti-nestin	Chemicon	Cat# ST1111-100UL RRID:AB_2043445
Mouse monoclonal anti-PSA-NCAM	Millipore	Cat# MAB5324 RRID:AB_11210572
Mouse anti-NeuN	Millipore	Cat# MAB377 RRID:AB_2298772
Rabbit anti-doublecortin	Sigma-Aldrich	Cat# SAB4500628 RRID:AB_10744013
Rabbit anti-nestin	Sigma-Aldrich	Cat# N5413 RRID:AB_1841032
Mouse monoclonal anti-GFAP	Sigma-Aldrich	Cat# WH0002670M1 RRID:AB_1841770
Guinea pig anti-doublecortin	Millipore	Cat# AB2253 RRID:AB_1586992
Rabbit anti-NeuN	Millipore	Cat# MABN140 RRID:AB_2571567
DyLight 594-AffiniPure Goat Anti-Rabbit IgG	Jackson ImmunoResearch Labs	Cat# 111-515-006 RRID:AB_2338042
Goat anti-Mouse IgG Secondary Antibody, Alexa Fluor 488	Thermo Fisher Scientific	Cat# R37120 RRID:AB_2556548
Goat anti-Mouse IgG Secondary Antibody, Alexa Fluor 488	Thermo Fisher Scientific	Cat# R37120 RRID:AB_2556548
DyLight 405-AffiniPure Goat Anti-Guinea Pig IgG	Jackson ImmunoResearch Labs	Cat# 106-475-003 RRID:AB_2337432
Goat anti-Mouse IgG Secondary Antibody, Alexa Fluor 488	Thermo Fisher Scientific	Cat# R37120 RRID:AB_2556548
Goat anti-Rabbit IgG Secondary Antibody, Alexa Fluor 594	Thermo Fisher Scientific	Cat# R37117 RRID:AB_2556545
Biological Samples		
Human hippocampal brain blocks	New York State Psychiatric Institute – Columbia University Medical Center Brain collection	https://www.columbiapsychiatry.org/research/research-divisions/molecular-imaging-and-neuropathology
Deposited Data		
Raw data	This paper	Available in Mendeley at https://doi.org/10.17632/7x9bbm324k.1

CONTACT FOR REAGENT AND RESOURCE SHARING

The authors plan to share materials and manage intellectual property according to the NIH Data Sharing Policy and Implementation Guidance updated March 5, 2003: https://grants.nih.gov/grants/policy/data_sharing/data_sharing_guidance.htm.

Sufficient experimental methods have been provided to facilitate accurate replication of the experiments, and we will respond to any questions regarding additional details of relevant protocols and published data. Material transfers will be made with no more restrictive terms than in the Simple Letter Agreement (SLA) or the Uniform Biological Materials Transfer Agreement (UBMTA) and without reach through requirements.

Should any intellectual property arise which requires a patent, we will ensure that the technology (materials and data) remains widely available to the research community in accordance with the NIH Principles and Guidelines.

The final dataset for this study, which includes demographic data, psychiatric assessment data, psychological ratings, and post-mortem studies data has been made available: https://doi.org/10.17632/7x9bbm324k.1. Because the data we collect are sensitive in nature, we carefully ensure that appropriate privacy safeguards are in place. All data are stripped of identifiers prior to release for sharing.

IRB materials including consent forms were written specifically to allow for the sharing of de-identified data with other investigators. We will make the data and associated documentation available to users under a data-sharing agreement that provides for: (1) a

commitment to using the data only for research purposes and not to identify any individual participant; (2) a commitment to securing the data using appropriate computer technology; and (3) a commitment to destroying or returning the data after analyses are completed.

Further information and requests for resources and reagents should be directed to and will be fulfilled by the Lead Contact, Maura Boldrini (mb928@cumc.columbia.edu).

EXPERIMENTAL MODEL AND SUBJECT DETAILS

Brain collection

Brain tissue was obtained from the Brain Collection of the New York State Psychiatric Institute at Columbia University, which includes brain samples from the Republic of Macedonia. Brain tissue collection was conducted with IRB approval and consent obtained from all informants.

Subject selection and matching procedure

All subjects are deceased. Our IRB has determined that this postmortem work is not Human Subjects Research. The only involvement of live individuals were as informants for Psychological Autopsy interviews. Subjects were diagnosed using our validated psychological autopsy for DSM axis I and II diagnoses. History of lifetime mood disorders and recent medication records were obtained. As part of the clinical evaluation, global functioning was measured by the Global Assessment Scale (GAS, score range 0-100, e.g.: 1-10 = danger of harming self or others, inability to maintain personal hygiene, or serious suicide attempt; 91-100 = no problems, or superior functioning in several areas, or admired by others due to positive qualities) as per DSM-IV Axis V (Roy et al., 1986). Recent (over the last two-month period) life event-associated stress (related to: primary support group, social environment, education, occupation, housing, finances, health, legal, or other psychosocial and environmental factors) was quantified using St. Paul-Ramsey Life Experience Scale (SPRS) total score and DSM-IV Axis IV severity (score range 1-7: none, minimal, mild, moderate, severe, extreme, catastrophic) (Endicott et al., 1976).

The subjects included in the study had no neurological or psychiatric diagnoses, no pathological or traumatic condition affecting the brain, clear toxicology reports, and were free of psychiatric treatments and cognitive impairment. Exclusion criteria were: any neuropsychiatric diagnosis, positive toxicology for psychoactive drugs or alcohol, alcoholism-associated liver changes, suicide attempt history, mental retardation, AIDS, chronic illness, positive neuropathology, undetermined death, resuscitation with prolonged (> 10min) hypoxia, received prescription of psychotropic medications in the last three months prior to death, long agonal states, and any chronic diseases. Subjects with the presence of diseases affecting the brain were excluded using clinical data, psychological autopsy interviews and neuropathological exams. Neuropathology excluded microvascular disease, including white matter lacunae. All subjects died by sudden death and the postmortem interval (PMI) was limited to 26 hours due to its effects on brain proteins (Roy et al., 1986). In addition, brains with damaged tissue or low pH were excluded.

The sample included 28 subjects, ages 14 to 79, consisting of 11 females and 17 males. Based on our previous studies on AHN and works from the literature, this sample size and age range was determined to have sufficient power to demonstrate statistically significant differences in prevalence of biomarker expression, neurogenesis, and angiogenesis with agin if they were to be present (Boldrini et al., 2009; Knoth et al., 2010; Ní Dhúill et al., 1999). When statistical analysis of the results was performed, there were no significant differences found between males and females with regards to expression of various biomarkers, angiogenesis or DG volume.

PMI ranged from 4 to 26 hours with no significant difference between aged and younger individuals. The subjects' cause of death included: 12 cardiovascular events, 11 traumatic deaths (homicide or motor vehicle accident), 2 bronchopneumonia, one accidental drowning, one uremia and one peritonitis (https://doi.org/10.17632/7x9bbm324k.1). All assays were performed in all 28 subjects except for double labeled immunofluorescence and stereology for Sox2/nestin and DCX/PSA-NCAM which were performed on three subjects age 20-29 and three subjects age 70-79 in order to assess differences between age groups. In order to avoid bias, the P.I. of the lab employed stratified randomization, using age as the confounding variable, when selecting which subjects would be used for the studies. Research assistants performing the experiments, imaging, stereology, and quantification of data were blind to the sex and age of the test subjects.

Brain tissue processing

At brain collection, 2 cm-thick coronal blocks of the right hemisphere were flash-frozen in liquid Freon (−20°C) and stored at −80°C. Tissue samples were fixed in formalin for neuropathological examination. Brain pH determination (Lewis, 2002) and toxicology were performed on cerebellar samples and blood. Over 30 drugs were screened for and quantified including amphetamine, cocaine, fluoxetine, sertraline, paroxetine, fluvoxamine, amitriptyline, nortriptyline, imipramine, citalopram, chlorimipramine, diazepam, alprazolam, buspirone, methadone, olanzapine, clozapine and haloperidol.

The hippocampal formation was dissected from frozen coronal blocks, fixed in 4% paraformaldehyde at 4°C, cryoprotected in 30% sucrose, sectioned at 50 μm on a sliding microtome (Microm HM440E) and stored in 40-wells boxes at −20°C in cryoprotectant (30% ethylene glycol in 0.1M PBS). One section every 500 microns was set aside for Nissl staining during the sectioning procedure. Nissl stained sections were later used for anatomical alignment along the DG rostro-caudal axis of sections processed for immunocytochemistry.

METHOD DETAILS

Immunocytochemistry

Immunocytochemistry was performed on serial sections at 2-mm intervals throughout the whole rostro-caudal extent of the DG. Sections were removed from the cryoprotectant and exhaustively washed in 0.01M Phosphate Buffer Saline (PBS) for 60 min (3 times 20'), then treated for 30 min with 0.5% sodium borohydride (Sigma-Aldrich, Saint Louis, MO) to remove aldehydes. Sections were subsequently rinsed in PBS and incubated for 10 min in PBS with 3% hydrogen peroxide (Sigma-Aldrich) to inhibit endogenous peroxidase activity. All procedures were performed at room temperature (RT) on a constantly rotating 55 rpm shaker.

Sections were then blocked in 20% (v/v) normal goat serum (Vector Laboratories, Burlingame, CA), 2% (w/v) Bovine Serum Albumin (Santa Cruz Biotechnology, Paso Robles, CA) and 0.3% (v/v) Triton X-100 (Sigma-Aldrich) prepared in PBS at RT for 1h.

Sections were incubated with the following primary antibodies: rabbit anti-Sox2 (1:1,000, Millipore, Billerica, MA), mouse anti-Ki-67 (1:200, Leica Biosystems, Newcastle Upon Tyne, UK), mouse anti-nestin (1:8,000, Chemicon, Temecula, CA), mouse anti-PSA-NCAM (1:2,000, Millipore) and mouse anti-NeuN (1:100,000, Millipore), rabbit anti-doublecortin (1:30000, Sigma-Aldrich, Millipore-Sigma, Temecula, CA) in a 1:10 dilution of the blocking solution for 3-5 days at 4°C on a shaker. Primary antibody was omitted in negative control sections. Sets of immediately adjacent sections were processed for each of the antibodies listed.

On day two, tissue sections were incubated for 2 hours at RT in biotin-conjugated secondary antibodies (anti-mouse, anti-rabbit or anti-guinea pig, Vector Laboratories), diluted 1:200 in 1% normal serum, 0.1% BSA and prepared in PBS. After washes with PBS, sections were incubated in avidin-biotin-horse radish peroxidase system (Vector Laboratories), diluted 1:200 in 1% normal goat serum and 0.1% BSA at RT for 1 hour. Sections were then washed and incubated in 0.05% 3,3′-Diaminobenzidine (DAB, Millipore Sigma), or Nickel-DAB, in 3% Hydrogen peroxide for 5 min, until color developed. Subsequently, sections were washed in sodium acetate for 10', followed by a PBS wash for 20' before being mounted on glass slides and desiccated. Differential staining was performed with Cresyl Violet (Nissl staining), Eosin or Nuclear Red, depending on the experiment. Lastly, sections were dehydrated in ethanol, clarified in Xylene, mounted with Permount (Sigma-Aldrich) and coverslipped.

Immunohistofluorescence

Immunohistofluorescence was performed by incubating sections in blocking solution with 0.3% Triton X-100 (Sigma-Aldrich), 10% normal goat serum (Vector Laboratories), 1%–2% bovine serum albumin (Santa Cruz) for 1 hour at RT. Subsequently, sections were incubated overnight, three days, or five days at 4°C in a 1:10 blocking solution with the following primary antibodies: 1:1,000 rabbit anti-nestin IgG (Sigma-Aldrich) and 1:25 mouse anti-Ki-67 IgG (Novocastra); 1:9,000 mouse monoclonal anti-GFAP antibody (Sigma-Aldrich) and 1:1,000 rabbit anti-nestin IgG (Sigma-Aldrich); 1:2,000 mouse anti-PSA-NCAM IgM antibody (Millipore) and 1:2,000 guinea pig anti-doublecortin IgG antibody (Millipore); 1:1,000 mouse anti-PSA-NCAM IgM antibody (Chemicon) and 1:500 rabbit anti-NeuN (Millipore); and 1:2,000 rabbit Sox2 IgG antibody (Millipore) and 1:2,000 mouse anti-nestin IgG antibody (Chemicon).

After overnight, three or five day incubation, tissue sections were incubated with secondary antibodies: 1:500 DyLight 594-AffiniPure goat anti-rabbit IgG (Jackson ImmunoResearch, West Grove, PA) and 1:500 goat anti-mouse IgG, Alexa Fluor 488 (Thermo Fisher Scientific); or 1:200 488-AffiniPure goat anti-mouse IgG and 1:200 594-AffiniPure goat anti-guinea pig IgG (Jackson ImmunoResearch); or 1:500 594-AffiniPure goat anti-mouse IgG and 1:500 488- AffiniPure goat anti-rabbit IgG (Jackson ImmunoResearch). Sections were treated with 0.1% Sudan Black in 70% ethanol for 5 minutes to reduce the innate auto-fluorescence of the human tissue; washed 3x15' in Tris buffer saline (pH: 7.6), mounted, dried overnight and coverslipped with ProLong Gold anti-fade reagent with DAPI (4',6-diamidino-2-phenylindole), a blue-fluorescent DNA stain that binds to dsDNA and is used as a nuclear counterstain in fluorescence microscopy (Invitrogen).

Replication

Due to the limited availability of human postmortem brain tissue, in comparison to the prevalence of rodent and other non-human tissues, it was not possible to replicate all the immunohistochemistry and immunohistofluorescence experiments. Rather, multiple hippocampus tissue sections containing the dentate gyrus were assessed for each subject, with an average of 10 sections per subject, spanning along the entire rostro-caudal extent of the dentate gyrus, which allowed applying unbiased stereology in order to estimate the total number of cells expressing each specific marker in the whole hippocampus of each subjects. We used adjacent series of sections across the entire rostro-caudal extent of the dentate gyrus, to perform experiments and stereology for each of the different markers and capillary measures, securing for the use of the same dentate gyrus regions across subjects and experiments. Before we determined the final optimal experimental and imaging protocols, several different experiments were run in trial tissue, and sections were imaged with different modalities, in order to determine optimum incubation times and concentration of primary antibodies, as well as the most reliable imaging conditions.

Confocal microscopy

Cell marker co-localization was analyzed by acquiring fluorescent confocal 3-dimensional z stack images and videos using an Olympus Fluoview FV1000 Confocal Laser Scanning System (Olympus, Waltham, MA) equipped with an Olympus IX81 Inverted Microscope, electronic stage controller (Prior Scientific, Rockland, MA), camera interface, and Olympus Fluoview 1000 (v. 1.5) software with the following objectives: UPLSAPO 10X and 20X air, with numerical aperture (NA) 0.40, 0.75; UPLFLN 40X oil with NA 1.30; and PLAFON 60X oil with NA 1.42 (Olympus). Briefly, the system is equipped with a 405-nm blue diode laser and multi-line (405, 488,

543 and 633 nm) argon ion laser (Melles Griot, Rochester, NY) as the excitation source. The Olympus Fluoview FV1000 has three confocal detectors and one transmitted light photomultiplier tube (PMT). The system is also equipped with a diffraction-grating based "spectral detection" system, and manual adjustment of wavelength detection for separation of signals from overlapping fluorophores. The fluorescence emitted was filtered by a BG39 filter set (Chroma, Rockingham, VT) and detected by a PMT (Hamamatsu, Bridgewater, NJ).

To quantify co-localization of cell markers (i.e., Sox 2/Nestin and DCX/PSA-NCAM), image stacks of the whole DG processed for immunohistofluorescence were obtained using a confocal scanning microscope (Leica TCS SP8 2-Photon, Leica Microsystems Inc.), and then processed for Stereology using Stereoinvestigator software (MBF, Inc.).

The Leica TCS SP8 2-Photon microscope is equipped with three simultaneous PMT detectors. Fluorescence from the different fluorophores was detected in the following way: 1) 488-AffiniPure was excited at 488 nm and detected at 505-550 nm, 2) 594-AffiniPure was excited at 552 nm and detected at 600-650 nm, and 3) DAPI was excited at 405 nm and detected at 415-485 nm. For 488- and 552-nm excitation, the beam path included a TD 488/552/638 beamsplitter, while for 405 nm excitation a substrate beamsplitter was used.

Tiled z stacks of the entire hippocampus area were obtained by first imaging conjugated fields of view via an automated stage in conjunction with the Stage Overview function of the LAS X software (Leica Application Suite X 3.1.1.15751), and then by stitching the images with the merging algorithm provided with the software. In order to select the area of the hippocampus on each section, the Stage Overview function was utilized. This function allowed for the fast acquisition of a low-resolution preview scan of the entire tissue section containing the hippocampus, using a 10x objective, and next for selecting the regions of interest surrounding the dentate gyrus to be included in the final tiled z stacks.

Image stacks from each tissue section assayed for Sox2/Nestin and for DCX/PSA-NCAM, along the rostro-caudal axis of the hippocampus, obtained from each subject, were acquired applying the same parameters to the Leica TCS SP8 2 photon microscope (Leica Microsystems Inc.). All z stacks were imaged with a dry Leica 20X objective (NA 0.70, working distance 0.5 mm), with a field of view of 553.6 × 553.6 μm, a pixel size of 0.54 × 0.54 μm, optical sectioning of 2.36 μm, and a z step of 1 μm. Depending on the thickness of each tissue section, the final z stack was determined to be 13 ± 2 μm. Image stacks were then imported in our MicroBrightfield system (MBF Bioscience, Williston, VT) to perform unbiased stereology.

Stereology

We used an unbiased stereological approach (optical *disector* with fractionator) to estimate cell numbers, capillaries, and DG volume. The system is equipped with Olympus BX51-WI microscope platform configured for neuronal reconstruction, Neurolucida software for 2D and 3D reconstruction, and Stereo Investigator stereology software for estimation of total cell numbers in the selected region of interest (MBF Bioscience, Williston, VT) in bright-field and immunofluorescence microscopy, and includes 4x, 10x, 20x, UPlan Fluorite, 40x air, 60x oil, 100x oil Plan Apo objectives, swing condenser, and achromatic aplanatic condenser, electronic stage controller LUDL MAC 6000 XYZ (BioVision Technologies, Exton, PA) and camera interface for Retiga 2000R CCD Scientific Camera (Q-Imaging, Surrey, BC, Canada).

Immunostained sections along the rostro-caudal axis of the DG were matched with intercalated Nissl-stained sections using a stereoscope (Leica, Wild M3Z, Heerburg, Switzerland). To quantify each cell type and proliferating capillaries, the first hippocampus slide to be sampled was the one in which the DG first appeared. Subsequent sections were assayed every 2.0 mm thereafter in systematic fashion, until the DG disappeared, with an average of 10-12 sections per subject. Using the Stereo Investigator system, DG boundaries were defined at low magnification using the 4x objective. Cells and capillaries were not counted in the upper and lower 3 μm in the z planes of the tissue sections (which were considered safety guard zones).

The estimated total number of cells was calculated as:

$$N = \sum Q^{-} \times \left(\frac{t}{h}\right) \times \left(\frac{1}{asf}\right) \times \left(\frac{1}{ssf}\right)$$

where Σ^{Q-} is the total number of cells counted, *t* is the mean section thickness, *h* is the height of the optical *disector* which adjusts for the guard zones above and below the dissector, *asf* represents the area sampling fraction (area of the counting frame divided by area of x,y step), and *ssf* is the section sampling fraction (1/section interval).

We assessed number of capillaries per mm^3, capillary area, length and bifurcations per capillary, which, taken together, represent the 3-D structure of the capillaries. For capillary area, a grid with tessellation points was randomly positioned on the same sections on which nestin+ cells were counted and the area was determined based on the number of grid points that were randomly laid over blood vessels by the Stereo Investigator software (MBF Biosciences). To measure capillary length and number of bifurcations per capillary we used the tracing tool of Neuroucida software (MBF Bioscience). The number of capillary bifurcations was calculated counting every bifurcation found on each capillary while tracing the capillary length, following capillary structures into the thickness of the tissue (sections were 50μm thick). The tracing tool calculates the length of the capillary while moving through it. Capillary volume was previously measured using Neuroucida software (MBF, Inc.). The diameter of the tracing tool was adjusted to fit the area of the transversal section of the capillary which changes along the vessel, this way the volume of each vessel was calculated, However, we found these volume measurements less reliable than the other capillary measures employed for the study.

The volume of the DG and GCL-SGZ were determined in anterior, mid and posterior hippocampus separately, using the Cavalieri method (Harrison et al., 1995). The areas of the outlines defining the DG and GCL-SGZ were measured on each section and analyzed

for cell counting and capillary measures. The region volume was then calculated by the stereology software based on section thickness (50 μm), number of sections (variable between subjects) and distance between sections (2 mm). Outlines of the DG including SGZ, GCL and ML (Figure 3E) were aligned from the most rostral to the most caudal hippocampal sections (Video S4), and used to calculate volume of anterior, mid and posterior DG and SGZ-GCL. We defined the anterior DG as the portion from the most rostral appearance of the DG to the start of the lateral geniculate. The mid DG was defined as the portion going from the start of the lateral geniculate to the disappearance of the lateral geniculate, and the posterior DG was the region from the end of the lateral geniculate to the end of the caudal DG.

QUANTIFICATION AND STATISTICAL ANALYSIS

Data analysis was performed using SPSS (version 24 for Mac). Number of subjects analyzed was 28, and we analyzed an average of 10 hippocampus sections per subject, along the whole rostro-caudal (anterior-posterior) axis of the hippocampus. Reported N values are representing cell numbers estimated by stereology in the anterior, mid and posterior dentate gyrus, as well as number of capillaries per mm^3, capillary area, length and bifurcations per capillary in the anterior, mid and posterior dentate gyrus. To test correlations between cell numbers, DG volume, capillary measures, age, PMI, and brain tissue pH, we used Pearson linear regression, when data were normally distributed, and Spearman correlation coefficient based on the ranked values, when they were not normally distributed (only used for Sox2+ cells). Significance level was set at $p < 0.05$. If we did not have the whole anterior, mid or posterior hippocampus, we did not report data for that section of the DG for that subject due to the fact that the total number of elements measured or region volume could not have been accurately determined. Statistical results of experiments can be found in the Result section of the manuscript and in the Figures. Significance level was set at $p < 0.05$; error bars in Figure S1 represent SD.

DATA AND SOFTWARE AVAILABILITY

All raw data have been uploaded in Mendeley at https://doi.org/10.17632/7x9bbm324k.1. Please contact the lead author of this paper for questions on data analysis and interpretation and additional information relevant to manuscript preparation.